This article was downloaded by:
On: *23 January 2011*
Access details: *Access Details: Free Access*
Publisher *Taylor & Francis*
Informa Ltd Registered in England and Wales Registered Number: 1072954 Registered office: Mortimer House, 37-41 Mortimer Street, London W1T 3JH, UK

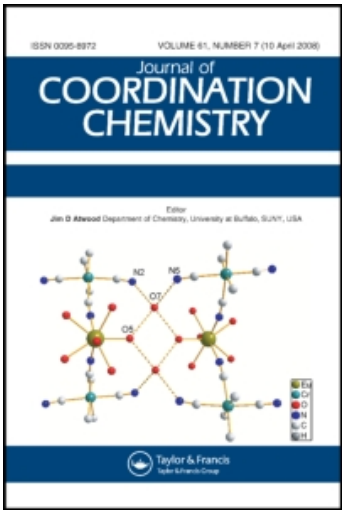

Journal of Coordination Chemistry
Publication details, including instructions for authors and subscription information:
http://www.informaworld.com/smpp/title~content=t713455674

Synthesis and characterization of 3-amino-5-methylisoxazole Schiff bases and their complexes with copper(II), nickel(II) and cobalt(II)

Shehab A. Sallam[a]
[a] Faculty of Science, Chemistry Department, Suez Canal University, Ismailia, Egypt

To cite this Article Sallam, Shehab A.(2007) 'Synthesis and characterization of 3-amino-5-methylisoxazole Schiff bases and their complexes with copper(II), nickel(II) and cobalt(II)', Journal of Coordination Chemistry, 60: 9, 951 — 971
To link to this Article: DOI: 10.1080/00958970600987990
URL: http://dx.doi.org/10.1080/00958970600987990

PLEASE SCROLL DOWN FOR ARTICLE

Full terms and conditions of use: http://www.informaworld.com/terms-and-conditions-of-access.pdf

This article may be used for research, teaching and private study purposes. Any substantial or systematic reproduction, re-distribution, re-selling, loan or sub-licensing, systematic supply or distribution in any form to anyone is expressly forbidden.

The publisher does not give any warranty express or implied or make any representation that the contents will be complete or accurate or up to date. The accuracy of any instructions, formulae and drug doses should be independently verified with primary sources. The publisher shall not be liable for any loss, actions, claims, proceedings, demand or costs or damages whatsoever or howsoever caused arising directly or indirectly in connection with or arising out of the use of this material.

Journal of Coordination Chemistry
Vol. 60, No. 9, June 2007, 951–971

Taylor & Francis
Taylor & Francis Group

Synthesis and characterization of 3-amino-5-methylisoxazole Schiff bases and their complexes with copper(II), nickel(II) and cobalt(II)

SHEHAB A. SALLAM*

Faculty of Science, Chemistry Department, Suez Canal University, Ismailia, Egypt

(*Received 16 May 2006; revised 6 July 2006; in final form 10 July 2006*)

Downloaded At: 11:44 23 January 2011

Schiff bases obtained by condensing 3-amino-5-methylisoxazole with salicylaldehyde, 2,3-dihydroxybenzaldehyde, 2,4-dihydroxy-benzaldehyde, 2,5-dihydroxybenzaldehyde or *o*-hydroxynaphthaldehyde were obtained and characterized by C, H, N analysis, mass, NMR and IR spectra. Copper, nickel and cobalt complexes of the Schiff bases were prepared and characterized using elemental analysis, conductivity measurements, magnetic moments, IR, UV-VIS and ESR spectra, X-ray diffraction, TGA, DTA and DSC thermal analysis. All the complexes are non-electrolytes. ESR spectra show isotropic as well as axial symmetry for the copper complexes. Thermal studies support the formulation of these complexes and showed that they decompose in two or three steps depending on the metal used. Activation energy E_a and enthalpies ΔH associated with the decomposition process were calculated and correlated with the complexed metal used.

Keywords: 3-Amino-5-methylisoxazole; Schiff bases; Complexes; Spectral and thermal properties

1. Introduction

Reactions of aldehydes and amines, including heterocyclic amines, are generally straightforward and give imines or Schiff bases [1–4]. However, when 2-amino-4-methyloxazole was reacted with aldehydes, no Schif fbases were formed [5]. Instead, products having free amino groups were obtained and were identified as oxazole-5-hydroxymethyl derivatives [6].

In this article we have synthesized and characterized Schiff bases obtained by condensing 3-amino-5-methylisoxazole with: salicylaldehyde, 2,3-dihydroxybenzaldehyde, 2,4-dihydroxy- benzaldehyde, 2,5-dihydroxybenzaldehyde or *o*-hydroxynaphthaldehyde. Complexes of Cu(II), Ni(II) and Co(II) with the Schiff bases were prepared and characterized using elemental analysis, magnetic moments, conductivity measurements, spectral (UV-VIS, ESR, X-ray diffraction) and thermal analysis (TGA, DTA, DSC).

*Email: shehabsallam@yahoo.com

ISSN 0095-8972 print/ISSN 1029-0389 online © 2007 Taylor & Francis
DOI: 10.1080/00958970600987990

2. Experimental

2.1. *Materials*

3-amino-5-methylisoxazole, hydroxybenzaldehydes and *o*-hydroxy-naphthaldehyde were purchased from Fluka and were used as supplied. Other chemicals are reagent grade and used without further purification.

2.2. *Preparation of the ligands*

Schiff bases were synthesized by refluxing a mixture of 1 : 1 molar amounts of 3-amino-5-methylisoxazole with each of: salicylaldehyde; 2,3-dihydroxybenzaldehyde; 2,4-dihydroxybenzaldehyde; 2,5-dihydroxy-benzaldehyde and *o*-hydroxynaphthaldehyde in absolute ethanol on a water bath for 1 h. The products were filtered off, washed with EtOH, recrystallized from absolute EtOH and finally dried in a vacuum desiccator over anhydrous $CaCl_2$. The Schiff bases were fully characterized by their melting points, IR, NMR and mass spectra. The following Schiff bases were used in this study.

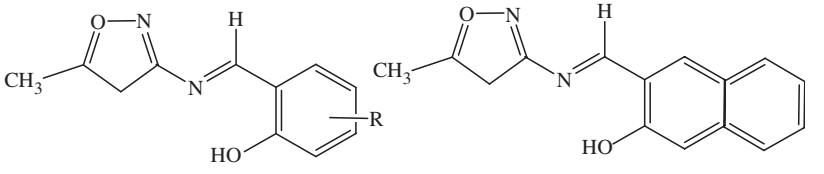

L^1: R= H; L^2 : R = 3-OH
L^3: R= 4-OH; L^4 : R = 5-OH

Downloaded At: 11:44 23 January 2011

2.3. *Preparation of the complexes*

The complexes were prepared by the addition of metal chlorides (0.01 mol) in EtOH (15 cm^3) to a hot EtOH solution of the ligands (0.02 mol). The mixture was heated under reflux with stirring for ½ h. The precipitated complexes were then removed by filtration, washed with EtOH and Et_2O and dried in vacuum.

2.4. *Physical measurements*

Elemental analyses for C, H and N were performed using a Heraus CHN-rapid analyzer. ^{1}H NMR spectra were obtained using a 200 MHz Varian-Gemini spectrophotometer using TMS as internal standard. The mass spectra of the Schiff bases were obtained with a Varian MAT-711 mass spectrometer. Metal analyses were carried out on an ARL 3410-ICP sequential spectrophotometer at wavelengths 324.75, 231.60 and 228.62 nm for Cu, Ni, and Co, respectively. The IR spectra were recorded (KBr disc) in the 4000–400 cm^{-1} range on a Nicolet Impact-400 and Bruker Vector-22 spectrophotometers. The electronic absorption spectra were obtained using nujoll mulls and

10^{-3} M DMSO or DMF solutions in a 1cm cell using a Beckman 5260 spectrophotometer. X-band ESR spectra were recorded on a Varian E4 spectrophotometer. Magnetic susceptibility measurements were carried out using the modified Gouy method on a Johnson–Matthey balance at room temperature using mercury(II)tetrathiocyanatocobaltate(II) as the calibrant. X-ray powder diffraction was performed using a Brucker Axs-D8 Advance diffractometer with Cu-Kα radiation. TGA, DTG, DTA and DSC were performed on a Perkin-Elmer Series7 thermal analyzer equipped with Pyres software under dynamic flow of nitrogen (10 L min^{-1}) and heating rate 10°C min^{-1} from ambient to 1000°C or 500°C (DSC). The number of decomposition steps was identified using DTG. Electrical conductivity measurements were carried out on freshly prepared 10^{-3} M DMSO solutions at room temperature using a WTW conductivity meter fitted with an L100 conductivity cell.

3. Results and discussion

3.1. *Characterization of the Schiff bases*

Reaction of 3-amino-5-methylisoxazole with some aromatic hydroxyaldehydes afforded the corresponding Schiff bases. Chemical analysis, melting points, mass spectra, DSC and TLC (using chloroform as eluent) confirm the purity of the synthesized Schiff bases (table 1). Infrared and ^{1}H NMR spectra are consistent with the expected structure as shown in tables 1 and 2. Mass spectral data showed the correct m/z corresponding to each reaction product.

The OH protons of L^1–L^5 Schiff bases come to resonance at $\delta = 11.8$, 11.5, 12.5, 11.2 and 14.4 ppm, respectively [2]. The broadening of the signals provides evidence for strong hydrogen bonding between phenolic or naphtholic hydroxyl group and the azomethine nitrogen forming a six-membered ring [7]. The azomethine protons appear as a singlet at $\delta = 9.5$ ppm for L^5 while the same signal resonates at $\delta = 8.83$ ppm for the rest of the compounds.

The significant infrared spectra of the Schiff bases are listed in table 2. All the Schiff bases give broad overlapping bands in the 3224–3448 cm^{-1} range, which may be attributed to the phenolic and naphtholic OH in the ortho- position with respect to the –C=N group. L^2 and L^4 give sharp bands at 3286 and 3279 cm^{-1}, which may be assigned to stretching vibration of the second OH groups present in the ortho- and para- positions with respect to the first OH group [2]. No absorption band υ(OH) is observed for L^3 Schiff base, indicating that the υ(OH) frequency is probably lowered to a considerable extent owing to strong intramolecular (OH$\cdots$N) and intermolecular (OH$\cdots$O) hydrogen bonding; quinonide formation should also be considered [8]. The high frequency sharp bands due to CH stretching frequencies observed in the 3116–3140 cm^{-1} range in the i.r. spectra of the Schiff bases are characteristic of the isoxazole ring [9]. Azomethine stretching vibrations appear as split bands with two maxima in the 1623–1601 and 1607–1570 cm^{-1} range for all Schiff bases due to the similarity of the Schiff base skeleton [10–11]. The fundamental stretching modes of the isoxazole ring occur between 1531 and 1362 cm^{-1} [8]. The bands in the region 1225–1282 cm^{-1} for the Schiff bases are ascribed to the phenolic and naphtholic C–O stretching vibration [12].

Downloaded At: 11:44 23 January 2011

Downloaded At: 11:44 23 January 2011

Table 1. Analytical data, melting points, mass and ^{1}H NMR.spectral values for the Schiff bases.

Ligand	Colour	Mol.wt.	M.p. (°C)	DTA peaks (°C)	m/z (%)	Found (Calcd)%			NMR data (ppm)	
						C	N	H	OH	N=CH
$C_{11}N_2O_2H_{10}$	Yellow	202.09	153	155	202.1 (84)	64.7 (65.1)	13.8 (13.8)	4.9 (4.9)	11.8	8.83
$C_{11}N_2O_3H_{10}$	Orange	218.09	185	188	218.1 (100)	60.3 (60.6)	12.6 (12.8)	4.5 (4.5)	11.5	8.83
$C_{11}N_2O_3H_{10}$	Light orange	218.09	143	154	218.1 (58)	60.1 (60.6)	12.7 (12.8)	4.5 (4.5)	12.5	8.83
$C_{11}N_2O_3H_{10}$	Yellowish orange	218.09	201	205	218.1 (89)	60.2 (60.6)	12.8 (12.8)	4.7 (4.5)	11.2	8.83
$C_{15}N_2O_2H_{10}$	Greenish yellow	252.13	194	196	252.0 (100)	71.0 (71.4)	11.1 (11.1)	4.7 (4.7)	14.4	9.5

Downloaded At: 11:44 23 January 2011

Table 2. Spectral data of the Schiff bases and their metal complexes.

Complex	IR spectral data (cm^{-1})						UV-VIS spectral data (cm^{-1})		
	$\upsilon_{(OH)}$	CH, CH_2, CH_3	$\upsilon_{(C=N)}$	Isoxazole ring mode	$\upsilon_{(C-O)}$	$\upsilon_{(M-N)}$ $\upsilon_{(M-O)}$	d–d bands		Intraligand and C.T.
L^1	3448 br.	3124, 3012,	1609	1499, 1451,1406, 1371	1279	–	Nujol	–	29,850, 36,363, 43,478
		2927, 2853	1574				DMF	–	30,303, 37,735, 40,000
$[CuL^1Cl(H_2O)_2]$	3445 br.	3147, 3057, 3015, 2922	1608	1526, 1442, 1400, 1360	1336	592	Nujol	12,903, 14,615	32,258, 41,666
			1578			436	DMF	12,560, 14,150	38,461
$[NiL^1ClH_2O] \cdot 2H_2O$	3346 br.	3200, 3078, 3051, 3023, 2878	1651	1528, 1464, 1411, 1361	1329	532	Nujol	16,129, 26,315	29,411, 35,714, 43,478
			1605			438	DMF	16,666, 26,315	40,000
$[CoL^1ClH_2O] \cdot 3½H_2O$	3418 br.	3142, 3118, 2929	1639	1530, 1479, 1436, 1375	1361	534	Nujol	16,000–16,528, 17,857	32,786, 37,735, 41,666
			1610			461	DMF	16,520, 18,310	30,780, 40,650
L^2	3377 br.	3132, 3002, 2924, 2737	1615	1497, 1461, 1406, 1365	1282	–	Nujol	–	29,411, 35,087, 45,454
	3286 sh.		1584				DMF	–	28,571, 35,460, 44,642
$[CuL^2(H_2O)_2]$	3416 br.	3144, 2925	1608	1527, 1437	1308	598	Nujol	16,949, 18,518	31,250, 41,666
						479	DMF	17,321, 23,255	30,210, 42,640
$[NiL^2(H_2O)_2] \cdot 3H_2O$	3358-	3061, 3032, 2971, 2863	1621	1550, 1506, 1458, 1393	1319	583	Nujol	17241, 23809	30,769, 41,666
			1550			482	DMF	18,223, 22,917	33,790, 40,512
$[CoL^2(H_2O)_2] \cdot 4H_2O$	3406 br.	3138, 3074, 2852	1619	1542, 1451, 1435, 1404	1314	540	Nujol	12,520, 16,666	30,461, 43,478
			1578			480	DMF	13,710, 17,857	31,500, 42,610
L^3	–	3126, 3074, 2924, 2767	1601	1531, 1508, 1476, 1425, 1381	1225	–	Nujol	–	23,809, 31,746, 42,553
			1570				DMF	–	31,055, 34,482, 44,052
$[CuL^3(H_2O)_2] \cdot 2H_2O$	3422 br.	3152, 3023, 2926	1617	1409, 1340	1266	540	Nujol	17,857, 19,607	26,315, 40,816
			1560			483	DMF	17,543, 20,000	31,250, 47,619
$[NiL^3(H_2O)_2] \cdot 3H_2O$	3299 sh.	3016, 2942, 2911, 2846	1610	1534, 1452, 1421, 1385	1254	539	Nujol	17,857, 23,255	30,303, 44,444
						485	DMF	17,830, 32,770	29,930, 43,234
L^4	3402 br.	3140, 3039, 2974, 2928	1616	1521, 1482, 1451, 1374	1257	–	Nujol	–	27,397, 35,087, 41,666
	3279 sh.		1587				DMF	–	31,055, 34,482, 44,052
$[CuL^4(H_2O)_2]$	3365 br.	2903, 2833	1609	1542,1498,1443,1377	1270	582	Nujol	12,987, 20,000, 23,255	29,411, 41,666, 43,478
			1542			479	DMS	12,563, 23,255	92,112, 42,356, 44,321
$[NiL^4(H_2O)_2] \cdot 3H_2O$	3299 br.	3048, 2959, 2903, 2846	1611	1535, 1454, 1421, 1386	1283	539	Nujol	17,857, 22,988	30,303, 42,553
						485	DMF	17,725, 23,130	31,234, 41,945
$[CoL^4(H_2O)_2] \cdot 2H_2O$	3278 br.	3140, 2982, 2935, 2862	1622	1540, 1492, 1453, 1377.	1272	579	Nujol	12,970, 17,857	30,303, 37,037, 47,619

(*continued*)

Downloaded At: 11:44 23 January 2011

Table 2. Continued.

Complex	IR spectral data (cm^{-1})						UV-VIS spectral data (cm^{-1})		
	$\upsilon_{(OH)}$	CH, CH_2, CH_3	$\upsilon_{(C=N)}$	Isoxazole ring mode	$\upsilon_{(C-O)}$	$\upsilon_{(M-N)}$ $\upsilon_{(M-O)}$	d–d bands		Intraligand and C.T.
			1588			486	DMF	12,640, 17,645	29,830, 36,760, 45,118
L^5	3224 br.	3116, 3058, 2923, 2740	1623	1516, 1480, 1443, 1415, 1362	1250	–	Nujol	–	27,027, 31,250, 45,454
			1607				DMF	–	27,397, 31,446, 40,000
$[CuL^5Cl(H_2O)_3]\cdot \frac{1}{2}H_2O$	3523 br.	3143, 3043, 2925	1619	1537, 1456, 1428, 1401, 1370	1306	570	Nujol	16,129, 25,000	38,461
			1605			499	DMF	16,345, 25,316	28,169, 33,333, 48,780
$[NiL^5ClH_2O]\cdot 2H_2O$	3339 br.	3188, 3059, 2925, 2890	1641	1539, 1460, 1429, 1397, 1367	1305	519	Nujol	16,750, 25,641	33,333, 40,000, 45,454
			1609			455	DMF	16,910, 26,150	34,120, 42,330, 47,120
$[CoL^5Cl(H_2O)_2]\cdot 2H_2O$	3402 br.	3171, 2923, 2837	1640	1538, 1459, 1427, 1394, 1366	1304	515	Nujol	17,543, 21,505	26,666, 37,735, 47,619
			1603			456	DMF	17,987, 23,809	29,850, 37,735, 44,3478

3.2. *Complexes of the Schiff bases*

All the complexes are insoluble in water and common organic solvents (methanol, ethanol, benzene, chloroform, acetone, dichloroethane and diethyl ether) but partly soluble in DMSO and DMF. The analytical data (table 3) show the following formulae for the complexes: $[ML^{1,5}Cl(H_2O)_n]xH_2O$, $n = 1, 2$, $x = 0$–$3\frac{1}{2}$ or $[ML^{2,3,4}(H_2O)_2]xH_2O$, $x = 0$–4 where $M = Cu^{II}$, Ni^{II} and Co^{II}. The molar conductance values in DMSO lie in the 2–20 μS range for all the complexes which indicate their non-electrolyte character [13] and that the anion is also coordinated to the metal ion. All the complexes were stable at room temperature and non-hygroscopic in nature. The 1 : 1 stoichiometries of the complexes have been concluded from their elemental analyses (table 3). The presence of coordinated water was confirmed by TGA data.

3.2.1. Infrared spectra. Infrared spectra of the complexes have been assigned for those principal bands i.e., υ(OH), υ(C=N) and υ(C–O) (table 2). The ligands band υ(OH) disappear in the spectra of the complexes, commensurate with displacement of the hydrogen proton upon complexation indicating bonding of the metal ions to the phenolic OH after deprotonation [14]. The higher frequency band due to the azomethine group absorption is shifted after complexation suggesting coordination between the azomethine nitrogen atom and the metals. The lower frequency –C=N band appears to be coupled with the –C=C– stretching mode [15]. The absorption peaks due to C–O bonds observed in the 1225–1282 cm^{-1} region in the spectra of the free ligands shift to higher wavenumbers and become less intense in the spectra of the complexes. The blue shift observed in the stretching frequencies of the isoxazole ring in the complexes compared to the free Schiff-bases can be attributed to the perturbing effect of the chelated metal ions. The presence of coordinated water molecules in all the complexes is indicated by a broad band in the 3278–3523 cm^{-1} range and two somewhat weaker bands around 850 and 700 cm^{-1}, which could be assigned to OH stretching, rocking and wagging vibrations, respectively [16]. Low frequency bands in the 592–515 and 499–436 cm^{-1} range are assigned to υ(M–N) and υ(M–O) stretching frequencies [17]. A stable six-membered chelate ring is formed by complex formation with azomethine nitrogen –C=N (and not the nitrogen of the pyrazole ring) and the ortho-phenolic or naphtholic OH group.

3.2.2. Magnetic and spectral properties. Visible spectra and magnetic moments of the various complexes were used to study the geometrical configuration of the metal(II) ions (tables 2 and 3).

The effective magnetic moments of the copper complexes lie in the 1.36–1.89 B.M. range which is fairly close to those observed for copper complexes with one unpaired electron, $[e_g^6 \cdot t_{2g}^3]$. Low values for the complexes $[CuL^2(H_2O)_2]$, $[CuL^3(H_2O)_2] \cdot 2H_2O$ and $[CuL^4(H_2O)_2]$ are indicative of some extended interaction in these complexes [18].

The significant electronic absorption bands in the spectra of the complexes recorded in nujol mull and in DMF solution are presented in table 2. The nujol mull spectrum of $[CuL^5Cl(H_2O)_3] \cdot \frac{1}{2}H_2O$ has a broad band at 16,129 cm^{-1} that can be assigned to $^2E_g \rightarrow {}^2T_{2g}$ transition with a shoulder at 25,000 cm^{-1}, indicating the copper(II) ion has octahedral geometry [19]. The nujol spectrum of the $[CuL^1Cl(H_2O)_2]$ complex has absorptions at 12,903 and 14,615 cm^{-1} which can be ascribed to $E'' \rightarrow A_1'$ and $E' \rightarrow A_1'$

Downloaded At: 11:44 23 January 2011

Downloaded At: 11:44 23 January 2011

Table 3. Analytical data, melting points, conductivity values and magnetic moments of the complexes.

Complex	Color	Mol.wt.	M.p. (°C)	Found (Calcd)%				Ω (μS)	μ_{eff} B.M.
				C	N	H	M		
$[CuL^1Cl(H_2O)_2]$	Deep olive	336.06	212	39.41 (39.31)	8.15 (8.33)	3.82 (3.86)	18.12 (18.90)	2	1.88
$[CuL^2(H_2O)_2]$	Deep brown	315.6	>400	41.53 (41.85)	8.81 (8.87)	3.8 (3.8)	19.98 (20.13)	5.5	1.36
$[CuL^3(H_2O)_2]\cdot 2H_2O$	Brown	351.6	>400	37.22 (37.57)	7.84 (7.96)	4.27 (4.55)	18.26 (18.07)	20	1.4
$[CuL^4(H_2O)_2]$	Deep brown	315.6	>400	41.39 (41.85)	8.51 (8.87)	3.53 (3.81)	20.61 (20.13)	12	1.57
$[CuL^5Cl(H_2O)_3]\cdot \frac{1}{2}H_2O$	Olive	413.08	228	47.93 (48.04)	7.43 (7.4)	4.11 (4.23)	15.56 (15.38)	9.5	1.89
$[NiL^1ClH_2O]\cdot 2H_2O$	Bright olive	349.2	>400	37.57 (37.83)	8.41 (8.01)	4.62 (4.29)	16.43 (16.80)	2.3	3.46
$[NiL^2(H_2O)_2]\cdot 3H_2O$	Shining olive	364.72	372	36.63 (36.22)	7.81 (7.67)	4.61 (4.93)	16.45 (16.09)	7.2	Dia.
$[NiL^3(H_2O)_2]\cdot 3H_2O$	Shining brown	364.72	386	36.86 (36.22)	7.45 (7.67)	4.49 (4.93)	16.17 (16.09)	18.1	Dia.
$[NiL^4(H_2O)_2]\cdot 3H_2O$	Shining brown	364.72	398	36.72 (36.22)	7.71 (7.67)	4.96 (4.93)	16.27 (16.09)	9.2	Dia.
$[NiL^5ClH_2O]\cdot 2H_2O$	Olive	399.24	320	34.22 (34.27)	7.63 (7.26)	4.22 (4.25)	15.34 (15.22)	11.1	3.71
$[CoL^1Cl.H_2O]\cdot 3\frac{1}{2}H_2O$	Sky blue	376.42	210	35.18 (35.09)	7.32 (7.43)	4.79 (4.78)	15.51 (15.66)	15.3	4.17
$[CoL^2(H_2O)_2]\cdot 4H_2O$	Brown	382.95	322	34.89 (34.49)	7.63 (7.31)	4.69 (4.70)	15.64 (15.38)	8.1	3.61
$[CoL^4(H_2O)_2]\cdot 2H_2O$	Deep brown	346.97	>400	38.51 (38.07)	8.32 (8.06)	3.38 (3.45)	16.42 (16.98)	7.6	3.37
$[CoL^5Cl(H_2O)_2]\cdot 2H_2O$	Bright yellow	417.47	330	43.45 (43.15)	6.72 (6.70)	4.49 (4.55)	14.03 (14.11)	9.1	4.55

transitions of Cu(II) ions in a five-coordinate trigonal bipyramidal geometry [15]. A distorted tetrahedral structure with $^2B_2 \rightarrow {}^2E$ transition at 16,949 and 17,857 cm^{-1}, and the $^2B_2 \rightarrow {}^1A_1$ transition at 18,518 and 19,607 cm^{-1} was proposed for $[CuL^2(H_2O)_2]$ and $[CuL^3(H_2O)_2]\cdot 2H_2O$ [15]. The bands at 12,987, 20,000 and 23,255 cm^{-1} for $[CuL^4(H_2O)_2]$ are assigned to $^2B_{1g} \rightarrow {}^2B_{2g}$, $^2B_{1g} \rightarrow {}^2A_{1g}$ and $^2B_{1g} \rightarrow {}^2E_g$ transitions of square–planar geometry [19].

The magnetic moments of the complexes $[NiL^1ClH_2O]\cdot 2H_2O$ and $[NiL^5ClH_2O]\cdot 2H_2O$ (3.46 and 3.71 B.M.) probably indicate a tetrahedral structure [20]. The electronic spectra of the two complexes show two d–d bands in the 16,129–16,750 and 25,641–26,315 cm^{-1} range which can be assigned to $^3T_1 \rightarrow {}^3T_2$ and $^3T_1 \rightarrow {}^3T_1(P)$ transitions of tetrahedral or pesudotetrahedral structure [21, 22]. Square planar d^8 metal complexes are characterized by three spin-allowed d–d bands [19], $d_{xy}(b_{1g}) \rightarrow d_{x^2-y^2}$ (b_{1g}), $d_{z^2}(a_{1g}) \rightarrow d_{x^2-y^2}$ (b_{1g}) and $d_{xz,yz}(e_g) \rightarrow d_{x^2-y^2}$ (e_g) corresponding to $^1A_{1g} \rightarrow {}^1A_{2g}$, $^1A_{1g} \rightarrow {}^1B_{1g}$ and $^1A_{1g} \rightarrow {}^1E_g$ transitions. Of the three expected low energy ligand field (d–d) bands, corresponding to transitions from the three lower d-levels to the empty $d_{x^2-y^2}$ orbital, two are easily observed in the visible spectra of $[NiL^2(H_2O)_2]\cdot 3H_2O$, $[NiL^3(H_2O)_2]\cdot 3H_2O$ and $[NiL^4(H_2O)_2]\cdot 3H_2O$. These bands are observed in the 17,241–17,857 and 22,988–23,809 cm^{-1} range and can be considered $^1A_{1g} \rightarrow {}^1A_{2g}$ (υ_1) and $^1A_{1g} \rightarrow {}^1B_{1g}$ (υ_2) transitions of Ni(II) in square-planar structure. The ligand field band from $^1A_{1g} \rightarrow {}^1E_g$ is obscured by more intense bands of other origins.

The complexes $[CoL^1ClH_2O]\cdot 3\frac{1}{2}H_2O$ and $[CoL^5Cl(H_2O)_2]\cdot 2H_2O$ show magnetic moments of 4.17 and 4.55 B.M. indicating the presence of three unpaired electrons. The four coordinate blue [23] complex $[CoL^1ClH_2O]\cdot 3\frac{1}{2}H_2O$ has a characteristic multiple band in the 16,000–16,528 cm^{-1} range associated with a shoulder at 17,857 cm^{-1} which can be attributed to $^4A_2 \rightarrow {}^4T_1(P)$ transition of tetrahedral geometry [24]. The d–d broad band in the nujol spectra of $[CoL^5Cl(H_2O)_2]\cdot 2H_2O$ at 17,543 cm^{-1} with a shoulder at 21,505 cm^{-1} is characteristic of square-pyramidal and or distorted trigonal-bipyramidal structure with $^4A_2(F) \rightarrow {}^4A_2(P)$ transition [19]. The complexes $[CoL^2Cl(H_2O)_2]\cdot 4H_2O$ and $[CoL^4(H_2O)_2]\cdot 2H_2O$ have magnetic moments of 3.61 and 3.37 B.M. which are intermediate between values of square-planar and tetrahedral structures. This can result from spin equilibrium between low- and high-spin states [25, 26]. The spectra of both complexes give $^2B_{2g} \rightarrow {}^2E_g$ and $^2B_{2g} \rightarrow {}^2A_{1g}$ transitions in the 12,520–12,970 and 1666–17,857 cm^{-1} range concordant with square-planar structure [27].

The electronic spectra in DMF solutions of all complexes are very similar to those in nujol mull, indicating that DMF does not alter the geometry of the complexes.

3.2.3. ESR spectra. The room temperature polycrystalline *x*-band ESR spectra are shown in figure 1. The solid copper(II) complexes show spectra characteristic of the d^9 system. The $[CuL^2(H_2O)_2]$, $[CuL^3(H_2O)_2]\cdot 2H_2O$ and $[CuL^4(H_2O)_2]$ complexes show a similar isotropic pattern without any hyperfine lines with $g_{iso} = 2.12$, 2.13 and 2.122, respectively. These values indicate tetrahedral structures and tetragonal distortion around the copper(II) ion [28, 29].

The polycrystalline ESR spectrum of $[CuL^1Cl(H_2O)_2]$ complex shows g_x, g_y, g_z and g_{av} values of 2.25, 2.12, 2.04 and 2.14, respectively, indicating rhombic distortion. The *R* value of the complex $[R = (g_y - g_z) - (g_x - g_y) = 0.6] < 1$ with $g_x > g_y > g_z$ show that the unpaired electron is in a $d_{x^2-y^2}$ orbital of copper(II). The spectral features are

Downloaded At: 11:44 23 January 2011

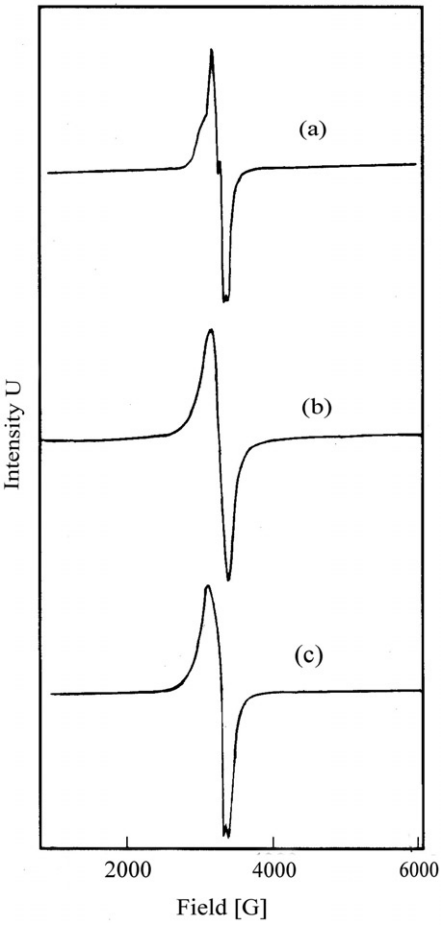

Figure 1. X-band powder ESR spectra of the copper complexes. (a) [CuL1Cl(H_2O)^2]. (b) [CuL^2(H_2O)$_2$]. (c) [CuL^5Cl(H_2O)$_3$] · ½H_2O.

characteristic of elongated tetragonally distorted square pyramidal copper(II) stereochemistry with all principle axes aligned parallel [30, 31]. For [CuL^5Cl(H_2O)$_3$] · ½H_2O, the ESR spectrum is characteristic of axial symmetry with $g_\parallel$, $g_\perp$ and g_{av} values of 2.33, 2.06 and 2.15. Anistropy of the g-tensor is due to the Jahn–Teller effect, which reduces the symmetry from O_h to D_{4h} [32]. The fact that $g_\parallel > g_\perp > \sim 2.0$ and $G = 5.5 > 4$ indicate octahedral geometry of the cooper(II) ion of $d_{x^2-y^2}$ ground state with negligible exchange interaction in the complex [31, 33].

3.2.4. X-ray powder diffraction. X-ray patterns of the complexes [CuL^2(H_2O)$_2$], [NiL^2(H_2O)$_2$] · 3H_2O, and [CoL^1(Cl)(H_2O)] · 3½H_2O were recorded over the $2\theta = 0$–100 range and are shown in figure 2. Generally, the [CuL^2(H_2O)$_2$] complex is amorphous while the [NiL^2(H_2O)$_2$] · 3H_2O and [CoL^1(Cl)(H_2O)] · 3½H_2O complexes

Downloaded At: 11:44 23 January 2011

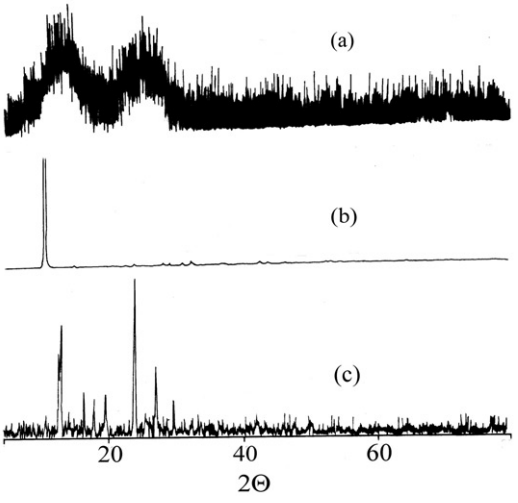

Figure 2. X-ray powder diffraction of some selected complexes. (a) $[CuL^2(H_2O)_2]$. (b) $[NiL^2(H_2O)_2] \cdot 3H_2O$. (c) $[CoL^1ClH_2O] \cdot 3\frac{1}{2}H_2O$.

Downloaded At: 11:44 23 January 2011

Table 4. X-ray powder diffraction of some selected complexes.

$[NiL^2(H_2O)_2] \cdot 3H_2O$						$[CoL^1ClH_2O] \cdot 3\frac{1}{2}H_2O$					
n	2Θ	*d*	*I*	Position	L* (nm)	*n*	2Θ	*d*	*I*	Position	L (nm)
1	10.18	8.67	100	10.1839	88.9	1	12.44	7.1	70.6	12.4835	56.0
2	14.47	6.11	0.6	14.5249	62.5	2	15.93	5.55	29.5	16.0297	89.5
3	23.83	3.73	0.6	23.7113	67.9	3	17.56	5.04	24.4	17.5661	94.4
4	28.47	3.13	0.3	28.0772	55.3	4	19.22	4.61	7.4	19.3531	49.8
5	32.29	2.76	1.0	28.8217	70.3	5	23.78	3.73	100	23.7466	85.8
6	36.96	2.42	0.2	30.735	83.4	6	27.01	3.29	45.4	25.4459	52.9
7	42.69	2.11	0.1	32.1357	107.7	7	29.84	2.99	24.0	27.0363	59.8
8	46.22	1.96	0.3	42.3229	104.2	8	77.21	1.23	7.6	29.796	132.4
				43.5685	92.2						
				53.0589	93.7						

*Crystal size.

are crystalline isomorphous. Each complex has specific (d) values, which can be used for its characterization (table 4) [34].

3.2.5. Thermal analysis. The thermal decomposition stiochiometries and dissociation enthalpies of the analytically characterized complexes were determined from their TGA, DTG, DTA and DSC curves. The activation energies of the decomposition reactions were determined from the DTA calorigrams. The obtained values are listed in table 5, and were calculated using the formula of Piloyan [35]:

$$\ln \Delta t = \frac{C - E_a}{RT}$$

Downloaded At: 11:44 23 January 2011

Table 5. DTA. and DSC. data of the Schiff bases and their complexes.

Complex	Temp. rang t(°C)	DTA peak t(°C)	ΔH (J g^{-1})	E_a (J mol^{-1})	Temp. rang t(°C)	DSC peak t(°C)	ΔH (J g^{-1})	Process
L^1	81–128	90 endo.	–	–	–	–	–	Phase change
	148–167	155 endo.			144–155	152 endo.	162	Melting
	243–267	258 exo.			262–264	263 endo.	150	Decomposition
$[CuL^1Cl(H_2O)_2]$	212–233	217 exo.	–	199	199–205	202 exo.	−410	Melting
	508–700	608 exo.		121				Final decomposition
$[NiL^1ClH_2O]\cdot 2H_2O$	116–190	165 endo.		191	176–184	178 endo.	89	Dehydration
	361–400	380 endo.		417	360–396	376 endo.	190	Decomposition
$[CoL^1ClH_2O]\cdot 3\frac{1}{2}H_2O$	167–191	179 endo.	89	185	161–169	166 endo.	90	Dehydration
	215–306	259 exo.	−722	100	205–266	242 exo.	−720	Coordination sphere
	499–766	624 exo.		56				Decomposition
L^2	179–184	188 endo.			173–176	175 endo.	151	Melting
	209–248	225 exo.			212–215	213 exo.	−176	Decomposition
$[CuL^2(H_2O)_2]$	50–181	99 endo.	443	79	96–121	107 endo.	129	Lattice rearrangement
	187–292	238 exo.	−336	143	171–238	213 exo.		Partial decomposition
	480–788	642 exo.	−397	–				Solid state reaction
$[NiL^2(H_2O)_2]\cdot 3H_2O$	368–409	386 endo.	210	73	359–376	368 endo.	375	Melting
	486–646	585 exo.	−893	116				Decomposition
	882–928	907 exo.	−362	205				Solid state reaction
$[CoL^2(H_2O)_2]\cdot 4H_2O$	239–350	284 exo.	–257	66	200–274	236 exo	−69	Coordination sphere
	503–627	560 exo.	−265	116	–	–	–	Decomposition
	700–873	756 exo.	−822	224				Solid state reaction
L^3	64–95	72 endo.	–	–	–	–	–	Phase change
	144–171	154 endo.			146–151	150 endo	148	Melting
	211–238	226 endo.			–	–	–	Lattice rearrangement

Downloaded At: 11:44 23 January 2011

	240–267	257 exo.			309–352	346 exo.	−174	Decomposition
$[CuL^3(H_2O)_2]\cdot 2H_2O$	55–181	114 endo.	903	208	112–140	123 endo.	285	Dehydration
	172–275	210 exo.	−579	232				Partial decomposition
	441–650	513 exo.	−286	108				Final decomposition
$[NiL^3(H_2O)_2]\cdot 3H_2O$	381–427	396 endo	291	183	369–381	376 endo	459	Melting
	531–607	568 exo.	−364	249				Decomposition
	851–880	870 exo.	−181	687				Solid state reaction
L^4	202–210	205 endo.			200–203	202 endo.	125	Melting
	210–232	216 exo.			203–210	206 exo.	−181	Decomposition
$[CuL^4(H_2O)_2]$	53–103	87 endo	133	63	67–97	85 endo	−349	Lattice rearrangement
	178–290	236 exo.	−430	47	152–246	202 exo.		Partial decomposition
	505–856	653 exo.						Final decomposition
$[NiL^4(H_2O)_2]\cdot 3H_2O$	384–428	400 endo.	335	55	374–385	380 endo	563	Melting
	487–605	554 exo.	−306	98				Decomposition
	841–881	866 exo.	−387	1413				Solid state reaction
$[CoL^4(H_2O)_2]\cdot 2H_2O$	222–335	263 exo	−418	53	200–251	225 exo.	−280	Coordination sphere
	475–605	580 exo						Decomposition
	789–840	816 exo.	−440	577				Solid state reaction
L^5	191–202	196 endo			201–205	204 endo.	110	Melting
	215–252	238 exo.			206–217	208 exo.	−150	Decomposition
$[CuL^5Cl(H_2O)_3]\cdot \frac{1}{2}H_2O$	109–163	136 endo.	99	132	123–149	151 endo.	89	Dehydration
	216–268	236 exo.	−209	202	197–225	214 exo.	−190	Coordination sphere
	589–715	665 exo.		–				Final decomposition
$[NiL^5ClH_2O]\cdot 2H_2O$	175–245	211 endo.	271	116	190–219	208 endo.	241	Dehydration
	313–412	352 endo.	415	122	323–325	324 endo.	333	Partial decomposition
	503–676	605 exo.	−530	133				Final decomposition
	856–909	892 exo.	−129	557				Solid state reaction
$[CoL^5Cl(H_2O)_2]\cdot 2H_2O$	133–199	170 endo.	266	93	173–188	184 endo.	196	Dehydration
	241–291	267 exo.	−41	232				Partial decomposition
	561–662	596 exo.	−115	565				Final decomposition

The plot of $\ln \Delta t$ *versus* $1000/T$ gave straight lines with a slop of $-E_a/RT$. ΔH of the decomposition steps for the complexes were calculated using the Pyres software supplied with the Perkin-Elmer thermal analyzer. The decomposition temperatures, the pyrolyzed products, the percentage mass loss of the complexes and the percent ash are given in table 6.

The melting points (table 1), of the ligands have the following order: $L^4 > L^2 > L^1 > L^3$, suggesting that thermal stability is influenced by variation in the substituent R (scheme 1). When $R =$ 3-OH and 5-OH the ligands have high stability while in L^3 the substituent $R =$ 4-OH has no effect on the thermal stability of the ligand. Thermal stability of the L^5 ligand is due to the presence of the bulky naphthalene ring.

The DTA of the ligands L^1 and L^3 show an endothermic peak in the temperature range 81–128 and 64–95°C with maxima at 90 and 72°C (table 5). These peaks could be attributed to phase transformations within the Schiff-base molecules. Melting of the ligands are shown by the sharp endothermic DTA peaks in the temperature range of 148–167, 179–184, 144–171, 202–210 and 191–202°C with maxima at 155, 188, 154, 205 and 196°C, respectively. Melting is confirmed by the sharp endothermic DSC peaks at 152, 175, 150, 202 and 204°C for L^1, L^2, L^3, L^4, and L^5, respectively. Ligand decomposition takes place in the temperature range 243–267, 209–248, 240–267, 210–232 and 215–252°C with sharp DTA exothermic peaks at 258, 225, 257, 216 and 238°C, respectively. L^3 has an endothermic DTA step following melting and before decomposition in the 211–238°C range with maximum at 226°C. This step is associated with colour change (thermochromism) from yellow to orange.

Downloaded At: 11:44 23 January 2011

Copper complexes

The complex $[CuL^1Cl(H_2O)_2]$ has a sharp decomposition step which starts at 175°C and ends at 218°C with a maximum rate at 195°C (table 6). The observed mass loss is 21.23% against calculated value of 21.25% showing that both the coordinated water and the chloride ion were expelled. With heating, the decomposition of the ligand continues with steady mass loss [44]. The thermal decomposition processes of $[CuL^2(H_2O)_2]$ and $[CuL^4(H_2O)_2]$ can be divided into three stages. The first stage occurs in the 100–181 and 173–256°C range with DTG peak at 166 and 228°C having mass loss of 10.85 and 10.09% (Calcd 11.4%) which corresponds to the loss of 2 mols of coordinated water. The second degradation stage is a continuation of the first, and occurs in the range of 181–286°C and 256–315°C with maximum rate observed at 276°C. The mass loss of 37.74 and 50.12% against calculated values of 38.02 and 50.69% shows partial decomposition of the ligand. The ligands in both complexes are completely removed at 314 and 396°C -with formation of copper metal- accomplished with a theoretical mass loss of 30.44 and 17.76%, which agrees with the experimental values of 31.82 and 19.27%.

The complex $[CuL^3(H_2O)_2] \cdot 2H_2O$ loses hydration water in the 76–184°C range with maximum rate at 141°C which correlates with mass loss of 10.6% (Calcd 10.23%). The second decomposition step starts at 226°C and ends at 334°C with DTG peak at 289°C concerning the evolution of two molecules of coordinated water and decomposition of the ligand. With heating, there is no clear plateau observed in the DTG curve of the complex, i.e. the intermediate product is unstable, continuing to lose mass with rising temperature.

Downloaded At: 11:44 23 January 2011

Table 6. TGA and DTG data of the complexes.

Complex	TGA plateau	DTG (°C)	Mass loss % (mg)		Process	Product	Residues % and type	
			Exp.	Calcd			Exp.	Calcd
$[CuL^1Cl(H_2O)_2]$	175–218	195	21.23	21.25	Coordination sphere	$2H_2O + L$	Not complete	
$[CuL^2(H_2O)_2]$	100–181	166	10.85	11.4	Coordinated water	$2H_2O$		
	181–286	276	37.74	38.02	Partial decomposition	0.55L	19.95	20.13
	286–345	314	30.82	30.44	Final decomposition	0.44L		Cu
$[CuL^3(H_2O)_2]\cdot 2H_2O$	76–184	141	10.6	10.23	Dehydration	$2H_2O$	Not complete	
	226–334	289	–	–	Decomposition	$2H_2O + L$		
$[CuL^4(H_2O)_2]$	173–256	228	10.09	11.40	Coordinated water	$2H_2O$		
	256–315	276	50.12	50.69	Partial decomposition	0.74L	19.47	20.13
	352–440	396	19.27	17.76	Final decomposition	0.26L		Cu
$[CuL^5Cl(H_2O)_3]\cdot \frac{1}{2}H_2O$	59–96	77	2.79	2.17	Dehydration	$\frac{1}{2}H_2O$		
	128–189	177	19.82	21.64	Coordination sphere	$3H_2O + Cl$		
	189–234	207	8.96	8.51	Partial decomposition	0.14L		
	234–293	249	5.2	4.86	Partial decomposition	0.08L	16.93	15.38
	356–478	408	45.47	46.81	Final decomposition	0.77L		Cu
$[NiL^1ClH_2O]\cdot 2H_2O$	76–144	121	10.48	10.3	Dehydration	$2H_2O$	21.13	21.38
	287–428	361	69.01	72.89	Decomposition	$H_2O + Cl + L$		NiO
$[NiL^2(H_2O)_2]\cdot 3H_2O$	237–320	309	15.03	14.79	Dehydration	$3H_2O$	19.47	20.47
	320–391	361	64.51	64.17	Decomposition	$2H_2O + L$		NiO
$[NiL^3(H_2O)_2]\cdot 3H_2O$	300–415	342	15.58	14.79	Dehydration	$3H_2O$	Not complete	
$[NiL^4(H_2O)_2]\cdot 3H_2O$	250–310	303	15.82	14.79	Dehydration	$3H_2O$	21.09	19.51
	310–384	333	63.62	64.17	Decomposition	$2H_2O + L$		NiO
$[NiL^5ClH_2O]\cdot 2H_2O$	100–160	130	10.03	9.01	Dehydration	$2H_2O$	17.99	18.70
	278–336	304	72.74	76.29	Decomposition	$H_2O + Cl + L$		NiO
$[CoL^1ClH_2O]\cdot 3\frac{1}{2}H_2O$	139–221	195	16.74	16.72	Dehydration	$3\frac{1}{2}H_2O$	20.13	21.33
	639–763	700	63.07	67.61	Decomposition	$H_2O + Cl + L$		Co_3O_4
$[CoL^2(H_2O)_2]\cdot 4H_2O$	71–189	151	19.14	18.79	Dehydration	$4H_2O$	Not complete	
	221–286	250	8.93	9.39	Coordinated water	$2H_2O$		
	463–584	520	–	–	Final decomposition	$H_2O + Cl + L$		
$[CoL^4(H_2O)_2]\cdot 2H_2O$	83–202	161	10.94	10.36	Dehydration	$2H_2O$		
	300–505	281	11.56	10.36	Coordinated water	$2H_2O$	18.07	18.5
	535–681	563	58.93	62.27	Final decomposition	L		Co_3O_4
$[CoL^5Cl(H_2O)_2]\cdot 2H_2O$	72–131	108	8.14	8.61	Dehydration	$2H_2O$		
	215–312	252	17.16	17.11	Coordination sphere	$2H_2O + Cl$	18.07	17.94
	515–571	537	54.01	60.01	Final decomposition	L		Co_3O_4

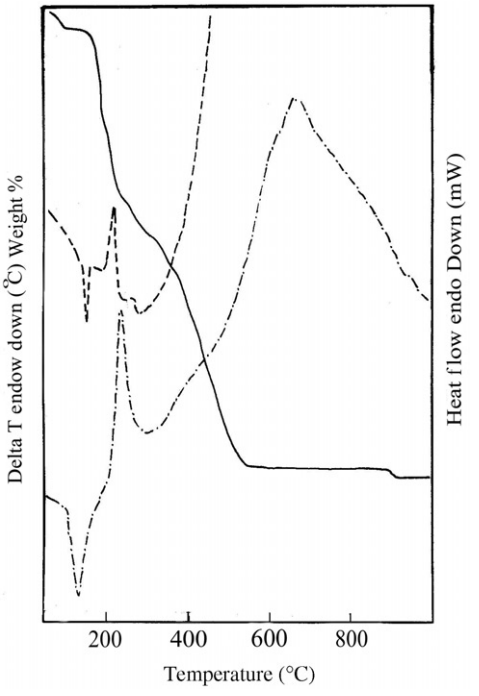

Figure 3. TGA —, DTA, -.-.- and DSC --- of $[CuL^5Cl(H_2O)_3]\cdot \frac{1}{2}H_2O$.

Downloaded At: 11:44 23 January 2011

A five step decomposition mechanism was proposed for $[CuL^5Cl(H_2O)_3]\cdot \frac{1}{2}H_2O$ (figure 3). The first step, dehydration of the complex, takes place in the range of 59–96°C with maximum at 77°C and mass loss of 2.79% (Calcd 2.17%). The second step starts at 128°C and ends at 189°C with DTG peak at 177°C and mass loss of 19.82% (Calcd 21.64%), which correlates to loss of 3 mols of coordinated water and the chloride ion. In the temperature range of 189–234°C, the third decomposition step takes place. It has a maximum DTG at 207°C with mass loss of 8.96% (Calcd 8.51%), from partial decomposition of the ligand. The fourth stage occurs between 234 and 293°C, corresponds to further decomposition of the ligand with the mass loss of 5.2% against the theoretical value of 4.86%. The maximum rate of loss is indicated by the DTG peak at 249°C. The final residue, estimated as copper metal is obtained at 408°C and has observed mass loss of 16.93% against the calculated value of 15.38%.

The DTA curve of $[CuL^1Cl(H_2O)_2]$ has two exothermic peaks. The first is sharp and takes place in the temperature range of 212–233°C with DTA peak at 217°C, which indicates melting of the complex [37]. This step is confirmed by the sharp exothermic DSC peak at 202°C, which takes place in the 199–205°C range. The second exothermic peak correlates with decomposition of the ligand, which occurs in the 508–700°C range with DTA peak at 608°C.

The DTA curves of $[CuL^2(H_2O)_2]$ and $[CuL^4(H_2O)_2]$ show one endothermic and two exothermic peaks. The endothermic one takes place in the 50–181 and 53–103°C range with DTA peaks at 99 and 87°C corresponding to lattice rearrangement. The DSC profiles of the complexes also show this step in the temperature range of 96–121 and

67–97 with endothermic peaks at 107 and 85°C. The first exothermic change occurs in the 187–292 and 178–290°C range with DTA peaks at 238 and 236°C, which correlates with decomposition of the coordination sphere. This step is also shown by the exothermic DSC changes in the 171–238°C and 152–246°C range with maxima at 213 and 202°C. Final decomposition is indicated by the broad exothermic DTA peaks at 642 and 653°C.

The DTA profiles of $[CuL^3(H_2O)_2]\cdot 2H_2O$ and $[CuL^5Cl(H_2O)_2]\cdot \tfrac{1}{2}H_2O$ show an endothermic effect in the 55–181 and 109–163 range with DTA peaks at 114 and 136°C representing dehydration. This is confirmed by endothermic DSC peaks taking place in the 112–140 and 123–149°C range with maxima at 123 and 151°C. Partial decomposition of these complexes occurs in the temperature range of 172–275 and 216–268°C with exothermic DTA peaks at 210 and 236°C. The complex $[CuL^5Cl(H_2O)_3]\cdot \tfrac{1}{2}H_2O$ shows this effect by a exothermic DSC peak in the 197–225°C range, with a maximum at 214°C. Final decomposition of the complexes is shown by the broad an exothermic DTA peaks at 513 and 665°C.

Nickel complexes

Downloaded At: 11:44 23 January 2011

Thermal decomposition of $[NiL^1ClH_2O]\cdot 2H_2O$ and $[NiL^5ClH_2O]\cdot 2H_2O$ takes place in two stages. The first stage starts at 76, 100°C and ends at 144, 160°C with DTG peak at 121 and 130°C. The corresponding mass loss of 10.48 and 10.03% (Calcd 10.03) and 9.01%) are due to volatilization of hydrated water. The second decomposition stage is well separated from the first and takes place in the 287–428 and 278–336°C range with maximum rate loss at 361 and 304°C. Mass loss of 69.01 and 72.74% (Calcd 72.89 and 76.29%) correlate with decomposition of the coordination sphere. The final residue, estimated as nickel oxide, has the observed mass of 21.13 and 17.99% against the calculated mass of 21.38 and 18.7%.

Based on the percentage of weight loss, the DTG curve and the complexation sustainment, consecutive two-step decomposition is proposed for $[NiL^2(H_2O)_2]\cdot 3H_2O$ and $[NiL^4(H_2O)_2]\cdot 3H_2O$ (figure 4). The first step occurs in the 237–320 and 250–310°C range with DTG peaks at 309 and 303°C corresponding to dehydration. The observed mass loss of 15.03 and 15.82% are consistent with the theoretical value of 14.79%. The second decomposition steps follow immediately after the first and take place in the temperature range of 320–391 and 310–384°C. The maximum rate mass loss is indicated by the DTG peak at 361 and 333°C, corresponding to degradation of two molecules of coordinated water and decomposition of the Schiff-base ligands. The observed mass loss of 64.51 and 63.62 coincide with calculated value of 64.17%.

The TGA-DTG curve of $[NiL^3(H_2O)_2]\cdot 3H_2O$, shows that decomposition starts at 300°C and ends at 415°C with maximum mass loss obtained by DTG at 342°C. The observed mass loss of 15.58% (Calcd 14.79%) is attributed to evolution of hydrated water. With heating, decomposition of the Schiff-base is continuous in the temperature range of 415–1000°C [36].

The DTA curves of $[NiL^2(H_2O)_2]\cdot 3H_2O$. $[NiL^3(H_2O)_2]\cdot 3H_2O$ and $[NiL^4(H_2O)_2]\cdot 3H_2O$ show sharp endothermic peaks in the 368–409, 381–427 and 384–428°C range with maximum at 386, 396 and 400°C, respectively indicating melting of the complexes. Sharp endothermic changes in the 359–376, 369–381 and 374–385°C range with DSC peaks at 368, 376 and 380°C confirm melting of the complexes. Decomposition of the complexes takes place in the 486–646, 531–607 and 487–605°C

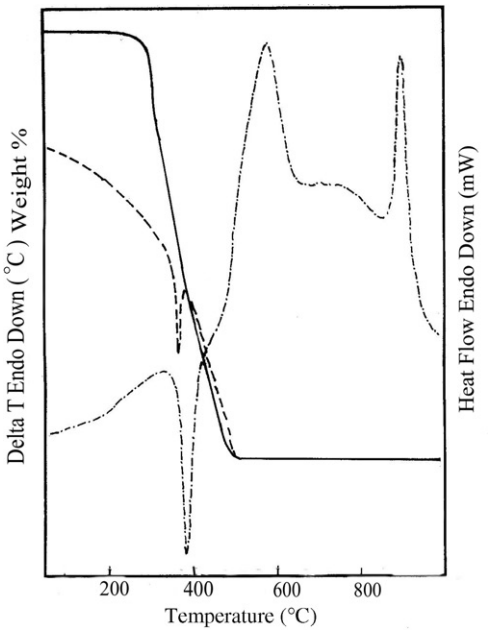

Figure 4. TGA ——, DTA -.-.- and DSC --- of $[NiL^2(H_2O)_2]\cdot 3H_2O$.

Downloaded At: 11:44 23 January 2011

range with exothermic DTA peaks at 585, 568 and 554°C, respectively. Solid-state reaction is shown by the exothermic DTA peaks at 907, 870 and 866°C.

Dehydration of $[NiL^1ClH_2O]\cdot 2H_2O$ and $[NiL^5ClH_2O]\cdot 2H_2O$ is indicated by the endothermic changes, which occur between 116–190 and 175–245°C with DTA peaks at 165 and 211°C. The DSC curves of these complexes have endothermic peaks at 178 and 208°C supporting dehydration. Thermal decomposition of the complexes induces endothermic changes in the temperature range 361–400 and 313–412°C with DTA peaks at 380 and 352°C. The DSC curves of these complexes show decomposition by endothermic peaks at 376 and 324°C. Final decomposition of $[NiL^5ClH_2O]\cdot 2H_2O$ is shown by the exothermic DTA peak at 605°C while the exothermic peak at 892°C indicates a solid-state mechanism.

Cobalt complexes

Decomposition of $[CoL^2(H_2O)_2]\cdot 4H_2O$, $[CoL^4(H_2O)_2]\cdot 2H_2O$ and $[CoL^5Cl(H_2O)_2]\cdot 2H_2O$ takes place in three stages. Water of hydration is evolved in the first stage 71–189, 83–202 and 72–131°C with DTG peaks at 151, 161 and 108°C, respectively. The mass loss observed are 19.14, 10.94 and 8.14% against calculated loss of 18.79, 10.36 and 8.61%, respectively. The second stage decomposition of $[CoL^2(H_2O)_2]\cdot 4H_2O$ and $[CoL^4(H_2O)_2]\cdot H_2O$ in the temperature range of 221–286 and 300–505°C with maximum rate loss at 250 and 281°C corresponds to loss of the coordinated water, with mass loss of 8.93 and 11.56% against the calculated values of 9.39 and 10.36%. The second decomposition stage of $[CoL^5Cl(H_2O)_2]\cdot 2H_2O$ takes place in the 215–312°C range with DTG peak at 252°C corresponding to evolution of the coordinated

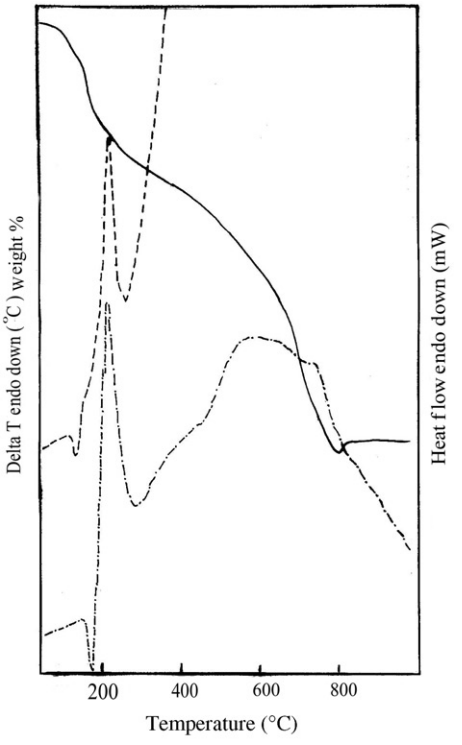

Figure 5. TGA ——, DTA -.-.- and DSC --- of $[CoL^1ClH_2O]\cdot 3\frac{1}{2}H_2O$.

Downloaded At: 11:44 23 January 2011

water and the chloride ion. The mass loss observed in this step is 17.16% against the calculated value of 17.11%. The third stage occurs in the temperature range of 463–584, 535–681 and 515–571°C with maxima at 520, 563 and 537°C, respectively, indicating final decomposition with the formation of Co_3O_4 as a final product. $[CoL^1ClH_2O]\cdot 3\frac{1}{2}H_2O$ decomposes in two steps (figure 5). The first starts at 139°C and ends at 221°C with maximum rate decomposition at 195°C with a mass loss of 16.74% (calculated 16.72%) corresponding to evolution of hydrated water. After 225°C, the complex shows a continuous weight loss with increasing temperature where the final decomposition takes place in the 639–763°C range with DTG peak at 700°C with the formation of Co_3O_4.

The complexes $[CoL^1ClH_2O]\cdot 3\frac{1}{2}H_2O$ and $[CoL^5Cl(H_2O)_2]\cdot 2H_2O$ dehydrate with endothermic changes in the 167–191 and 133–199°C range, associated with DTA peaks at 179 and 170°C. The DSC curves of the complexes support dehydration with endothermic peaks occurring in the 161–169 and 173–188°C range with maxima at 166 and 184°C. Decomposition of the coordination sphere of these complexes is shown by exothermic peaks in the 215–306 and 241–291°C range with DTA maxima at 259 and 267°C. This step is shown also by the DSC change in the 205–266°C range with an exothermic peak at 242°C for $[CoL^1ClH_2O]\cdot 3\frac{1}{2}H_2O$. Final decomposition is indicated by the exothermic DTA peaks at 624 and 596°C for both $[CoL^1ClH_2O]\cdot 3\frac{1}{2}H_2O$ and $[CoL^5Cl(H_2O)_2]\cdot 2H_2O$.

The complexes $[CoL^2(H_2O)_2]\cdot 4H_2O$ and $[CoL^4(H_2O)_2]\cdot 2H_2O$ have decomposition of the coordination sphere in the 239–350°C and 222–335°C range with exothermic

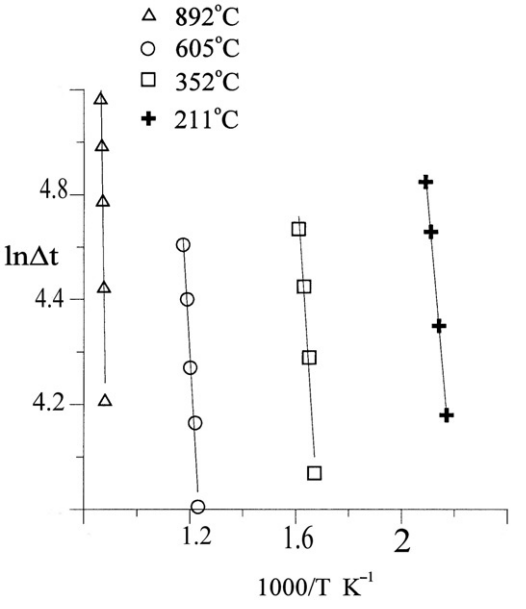

Figure 6. ln Δt *vs.* $1000/T$ relationship for $[NiL^5ClH_2O]\cdot 2H_2O$.

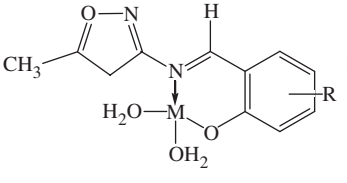

R=2–, 3–, 4–O^-; M=Cu(II), Ni(II),Co(II)

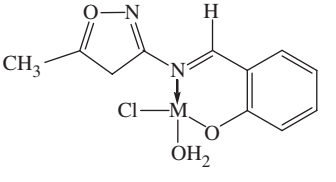

M=Ni(II), Co(II)

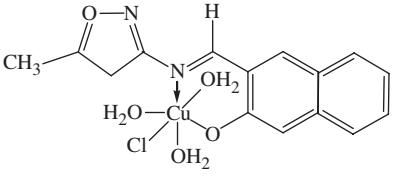

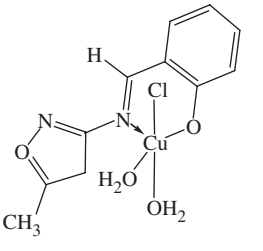

Scheme 2. Proposed structures.

DTA peaks at 284 and 263°C. The DSC curves of these complexes support this decomposition by exothermic peaks taking place in the 200–274 and 200–251°C range with maxima at 236 and 225°C. Final decomposition of the complexes takes place in the 503–627 and 475–605°C range with exothermic DTA peaks at 560 and 580°C. Solid-state reaction is indicated by exothermic peaks at 756 and 816°C.

The activation energy values for the Cu(II), Ni(II) and Co(II) complexes are expected to increase proportionally to the decrease in their atomic radius [38]. The activation

Downloaded At: 11:44 23 January 2011

energies of the first decomposition step for the complexes of Cu(II), Ni(II) and Co(II) with each of the ligands L^1; L^2; L^4 and L^5 are 199,191,185; 79,73,66; 63,55,53 and 132, 116, 93 J mol^{-1} (table 5). The ΔE_a values for each group of complexes are proportional to the metallic radius. The shorter the radius of the metal ion, the easier the approach of the ligand to the central atom. As a result, metal-ligand interaction becomes stronger, the detachment of the link more difficult and ΔE_a values increase [39, 40].

Based on the above analytical data and physicochemical properties the following structures are proposed in which the metal ion is coordinated through the azomethine nitrogen, oxygen of the ionized phenolic group, coordinated water and the chloride ion (scheme 2).

References

[1] H. Schiff. *Annls. Chem.*, **131**, 118 (1864).
[2] Sh.A. Sallam, A.S. Orabi. *Egypt. J. Chem.*, **47**, 383 (2004).
[3] Sh.A. Sallam. *Trans. Met. Chem.*, **30**, 341 (2005).
[4] Sh.A. Sallam. *Trans. Met. Chem.*, **31**, 46 (2006).
[5] H.R. Khan, G. Crank. *Tetrahedron Lett.*, **28**, 3381 (1987).
[6] H.R. Khan, G. Crank, S. Jesdapaulpaan. *J. Heterocycl. Chem.*, **25**, 815 (1988).
[7] H. Ranganathan, D. Ramaswamy, T. Ramasami, M. Santappa. *Chem. Lett.*, 201 (1979).
[8] H. Ranganathan, T. Ramasami, D. Ramaswamy, M. Santappa. *Indian J. Chem.*, **25A**, 127 (1986).
[9] L.J. Bellamy. *The Infra-red Spectra of Complex Molecules*, 3rd Edn, Chapman, Hall, London (1973).
[10] E.C. Okafer. *Spectrochim. Acta*, **38**, 981 (1982).
[11] K. Uneo, A.E. Martel. *J. Phys. Chem.*, **59**, 998 (1955).
[12] J.E. Kovacic. *Spectrochim Acta*, **23A**, 183 (1967).
[13] W.J. Geary. *Coord. Chem. Rev.*, **7**, 81 (1971).
[14] A. Saymal. *Trans. Met. Chem.*, **5**, 220 (1980).
[15] B.V. Batel, K. Desai, T. Thaker. *Synth. React. Inorg. Org.-Met. Chem.*, **19**, 391 (1989).
[16] M. Mohan, M. Kumar. *Polyhedron*, **4**, 1929 (1985).
[17] K. Nakamoto. *Infrared and Raman Spectra of Inorganic and Coordination Compounds*, 3rd Edn, John Wiley & Sons, New York (1992).
[18] M.A. Ali, S.E. Livingstone. *Coord. Chem. Rev.*, **13**, 101 (1974).
[19] A.B.P. Lever. *Inorganic Electronic Spectroscopy*, 2nd Edn, Elsevier, Amstrdam (1984).
[20] C.R. Hare, C.J. Ballhausen. *J. Chem. Phys.*, **40**, 788 (1964).
[21] A.B.P. Lever. *J. Inorg. Nucl. Chem.*, **27**, 149 (1965).
[22] S. Buffagni, L.M. Vellewrino, J.V. Quagliano. *Inorg. Chem.*, **3**, 480 (1964).
[23] K.C. Patel, P.R. Patel. *J. Inorg. Nucl. Chem.*, **39**, 1325 (1977).
[24] B.N. Figgis, R.S. Nyholm. *J. Chem. Soc.*, 338 (1959).
[25] K.K.M. Yusuf, A.R. Karthikeyan. *Trans. Met. Chem.*, **18**, 435 (1993).
[26] M. Goodgame, F.A. Cotton. *J. Am. Chem. Soc.*, **85**, 1543 (1962).
[27] K. Mukkanti, K.B. Pandeya, R.P. Singh. *Synth. React. Inorg. Met.-Org. Chem.*, **16**, 229 (1986).
[28] A.S. El-Tabl, M.M. Abou-Sekkina. *Polish. J. Chem.*, **73**, 1937 (1999).
[29] A.S. El-Tabl. *Trans. Met. Chem.*, **23**, 63 (1998).
[30] W. Fitzgerald, B.J. Hathaway. *J. Chem. Soc. Dalton Trans.*, 567 (1981).
[31] B.J. Hathaway, E.D. Billing. *Coord. Chem. Rev.*, **5**, 143 (1970).
[32] I.B. Bersuker. *Coord. Chem. Rev.*, **14**, 357 (1975).
[33] I.M. Proctor, B.J. Hathaway, P. Nocholis. *J. Chem. Soc.*, 1678 (1968).
[34] E.R. Souaya, W.G. Hanna, E.H. Isamil, N.E. Milad. *Molecules*, **5**, 1121 (2000).
[35] G.O. Piloyan, I.D. Ryabchikov, O.S. Novikova. *Nature*, **5067**, 1229 (1966).
[36] J.A. Dean (Ed.), *Langs Hand Book of Chemistry*, 13th Edn, McGraw-Hill, New York (1967).
[37] M. Gaber, M.M. Ayad, M.I. Ayad. *Therm. Acta*, **176**, 21 (1990).
[38] H. Arslan, N. Özpozan, N. Tarkan. *Therm. Acta*, **383**, 69 (2002).
[39] H. Sangari, G.S. Sodhi. *Therm. Acta*, **171**, 149 (1990).
[40] M.L. Kantouri, G.A. Katsoulos, C.C. Hadjikostas, P. Kokorotsikos. *J. Therm. Anal.*, **35**, 2411 (1989).

Downloaded At: 11:44 23 January 2011